16th World Conference on Earthquake, 16WCEE 2017
Santiago Chile, January 9th to 13th 2017
Paper N° 998
Registration Code: S-988

SLIDING DEFORMATION MODEL FOR REINFORCED CONCRETE SHEAR WALLS UNDER SEISMIC LOADING

B. Trost[1], H. Schuler[2], B. Stojadinovic[3]

[1] Research Associate, Institute of Civil Engineering, FHNW, Muttenz, burkhart.trost@fhnw.ch
Doctoral Student ETH, Zürich, trost@ibk.baug.ethz.ch
[2] Professor for Reinforced Concrete, Institute of Civil Engineering, FHNW, Muttenz, harald.schuler@fhnw.ch
[3] Professor for Structural Dynamics and Earthquake Engineering, ETH, Zürich, stojadinovic@ibk.baug.ethz.ch

Abstract

Accounting for all possible failure modes in seismic design and construction of reinforced concrete shear walls is important to ensure that the expected seismic performance of the building structures is attained. Sliding is a shear wall failure mode that can occur at flexural cracks or at cold joints. For example, significant sliding was observed at a four-story reinforced concrete building tested on the E-Defense shaking table [1]. Whyte [2], Synge [3] and Luna [4] observed and examined sliding failure in their squat shear wall tests.

In earthquake engineering, the sliding resistance on a crack in a reinforced concrete structural element is defined by simple equations in nearly all modern codes (EC8, ACI 318-1, fib-Model Code 2010). These equations have been developed for crack sizes occurring at serviceability performance levels and modified for use in seismic design. Large crack widths, which are common under earthquake loads, are not explicitly considered.

This article presents a sliding resistance and deformation model for reinforced concrete shear walls. This model includes the interaction between the concrete and the reinforcement and complies with the equilibrium of forces and the compatibility of deformations at each point in the sliding process. At the core of the model is a plastic micro-model that characterises the interlocking process of the aggregate on an existing crack. Depending on the concrete strength, the compression stress, and the roughness of the crack surface, the force transferred across the crack is determined for any displacement and any crack width. The model is validated against a series of sliding tests on compact sliding specimens (see Fig.1).

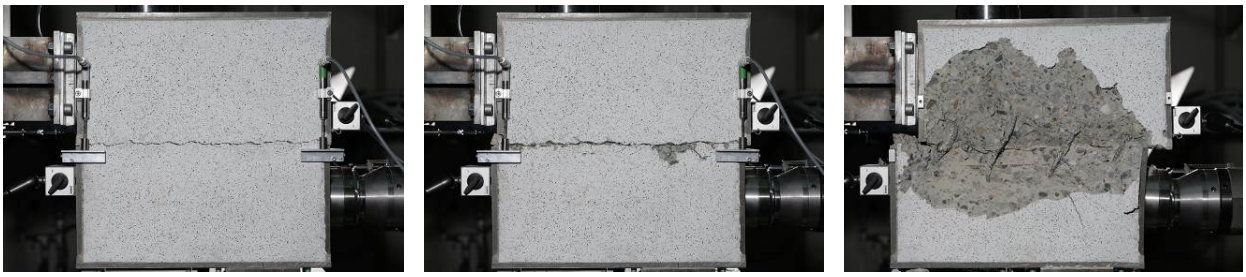

Fig.1 – Compact sliding specimen at 2 mm, 10 mm, and 50 mm displacement

Keywords: Sliding; Shear friction; Sliding shear; Shear walls; Aggregate interlock

1. Introduction

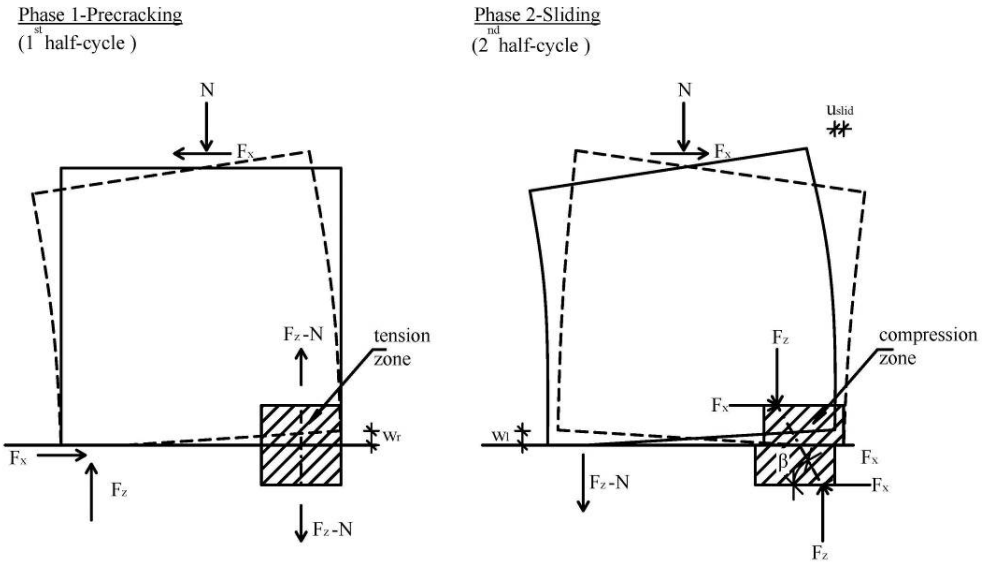

Fig.2 –Sliding of shear walls

The deformation behaviour of a cyclically loaded wall is shown in Fig.2. The hatched section of the wall is responsible for the sliding behaviour in the 2nd half-cycle. In the 1st half-cycle this section was located in the tension zone of the wall where a crack may open at a cold joint or at the section between wall and foundation. In the 2nd half-cycle, such crack may not fully close; nonetheless, the horizontal shear force is transferred across such open crack in the compression zone of the wall. This load deformation behaviour of the compression zone that was cracked in flexure earlier in the response history is responsible for the sliding behaviour of the wall.

2. Sliding model

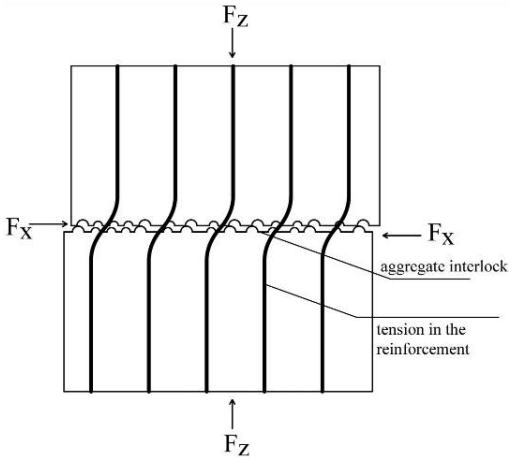

Fig.3 –Sliding model in the compression zone of a wall (Fig. 2)

A sliding model, comprised of an aggregate interlock model and a deflection model of the reinforcement, is developed to predict the sliding behaviour of shear walls under horizontal cyclic loads. The model describes the mechanical behaviour of reinforced concrete at a horizontal crack (see Fig.3). Aggregate interlock is modelled with an ideal plastic micro-model. The aggregate interlock effect depends on the crack width, the concrete strength, and the roughness of the crack surface. To describe the deformation behaviour of the

reinforcement, a deflection model is proposed. This model allows bending and axial deformation of the reinforcement at the crack. Both models are compatible in displacements and produce vertical and horizontal reaction forces at the crack. For a given sliding displacement, the model calculates the crack width needed to accomplish the equilibrium of forces and the compatibility of deformations.

2.1 Aggregate interlock model of cracked concrete

2.1.1 Mechanical approach

The aggregate interlock model is based on the model from Walraven [5], where sections of aggregate grains are assumed to be circular. The crack width is w, and the diameter of each aggregate, i, is d_i. The tensile strength is low at the surface between the aggregate and the cement matrix, so tension forces can induce cracks in the concrete. These cracks develop along the surfaces of the aggregate grains.

When two pieces of concrete, separated by a horizontal crack, are loaded by shear forces, sliding displacements, u_{slid}, are assumed to occur. A portion of the horizontal crack is geometrically defined in Fig.4. The grey-shaped circle represents the cross section of an aggregate grain, assumed to be a perfect sphere, and the hatched area shows the cement matrix. To reach this state of displacement, parts of the cement matrix must be plastically deformed (crushed), while the geometry of the aggregate remains unchanged. The stress acting at the contact surface between the aggregate grain and the cement, σ_{cu}, is perpendicular to the aggregate grain surface (radial to the sphere). To determine the plastic stress resistance, an equation from Walraven [5] is used (see Eq.(1)). No local shear stresses or friction are considered at the surface of the grains because of the roughness on the grain surface is assumed to be small and cement matrix is being destroyed (crushed) during the sliding process.

$$\sigma_{cu} = 6.39\, f_{cc}^{0.56}\ [N/mm^2] \tag{1}$$

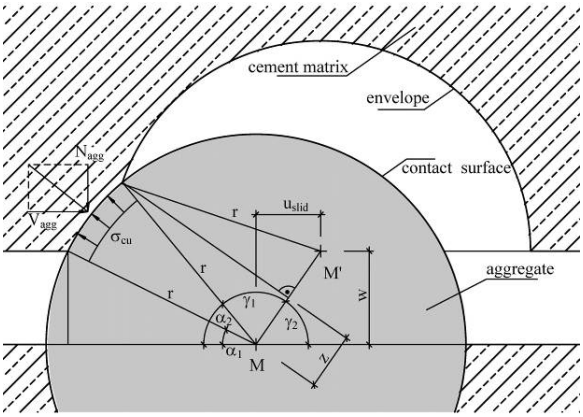

Fig.4 – Aggregate grain contact area

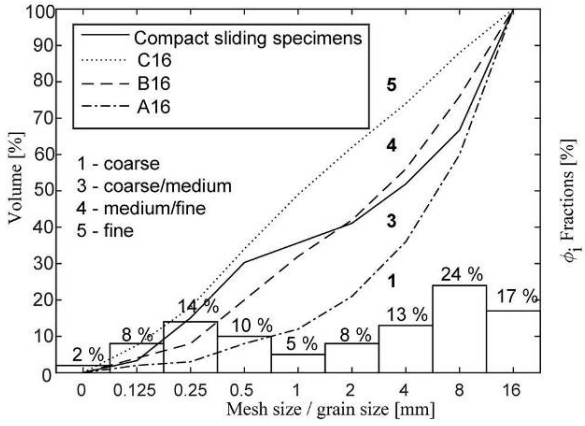

Fig.5 –Aggregate grain size distribution

The size of the contact surface depends on the diameter, d, of the grain, the sliding displacement, u_{slid}, and the crack width, w. Point M is the center of the aggregate grain in its location after sliding, and point M' is the center of the aggregate in its initial location. Then, u_{slid} is the horizontal distance between M and M'. The contact sector is between the angles α_1 and α_2. The first slip is assumed to occurs without contact between the aggregate grain and the cement matrix. Then, the aggregate grains with the largest diameter touch the cement matrix. For standard concrete, the compression strength of the aggregates is higher than that of the cement matrix. Because of this, the aggregate grains locally destroy the cement matrix. This leads to sliding displacements, but not automatically to a reduction of the sliding resistance. On the contrary, larger sliding displacements activate the smaller aggregate grains, which add to the sliding resistance.

For a single perfectly spherical grain loaded with a uniform radial stress, σ_{cu}, distributed along the contact sector between angles α_1 and α_2 and spanning the half of the sphere in contact with the cement paste the resultant shear force, V_{agg}, is calculated using Eq. (2) and the resultant normal force, N_{agg}, is calculated using Eq.(3). Each

equation is divided into two parts. The first part is the integration of the stresses to a resultant stress per circle section. This value is multiplied with the second part $(\pi d_i)/4$ to get the forces for a cylindrical grain that has the same area projected onto the crack surface as a spherical grain (see Fig.6). This assumption considers that half of the sphere is in contact with the cement between the angles α_1 and α_2 (Fig. 4).

$$V_{agg,i} = \left(\int_{\alpha_1}^{\alpha_2} \left(\frac{d_i}{2} \cdot \sigma_{cu} \cdot cos(\alpha) \right) d\alpha \right) \cdot \left(\frac{\pi}{4} \cdot d_i \right) \tag{2}$$

$$N_{agg,i} = \left(\int_{\alpha_1}^{\alpha_2} \left(\frac{d_i}{2} \cdot \sigma_{cu} \cdot \sin(\alpha) \right) d\alpha \right) \cdot \left(\frac{\pi}{4} \cdot d_i \right) \tag{3}$$

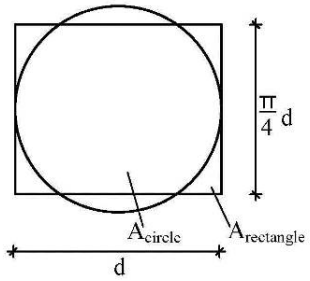

Fig.6 –View of the spherical and cylindrical grain projection onto the crack surface

The shear and the normal stresses transferred by each aggregate grain to the horizontal crack surface are modeled by dividing the grain forces V_{agg} and N_{agg} by the average area, A_{agg}, of the aggregate grain that crosses the horizontal crack surface.

$$\overline{\tau_{c,i}} = \frac{V_{agg,i}}{d_i^2 \cdot \frac{\pi}{4}} \tag{4}$$

$$\overline{\sigma_{c,i}} = \frac{N_{agg,i}}{d_i^2 \cdot \frac{\pi}{4}} \tag{5}$$

2.1.1 Crack Roughness and Aggregate Grain Size Distribution

The roughness of the crack is quantified using the aggregate grain size distribution in concrete. In the DIN 1045-2 [6], the aggregate grains size distributions A16, B16, and C16 separate the spectrum into four groups: fine, fine to medium, medium to coarse, and coarse (see Fig. 5). The solid line shows the grain size distribution that was used for the compact sliding specimens made in this study. This distribution is partially classified as coarse to medium, and partially as medium to fine. In the sliding model, the grain size distribution in the volume is considered to be equal to the distribution on the crack surface. Furthermore, the center of each grain is positioned at the surface of the crack (see Fig.4).

The contribution of each aggregate grain size to the stresses at the crack surface is computed separately and then summed together. For the concrete used in this study, the aggregate grain size diameter, d_i, were 16 mm, 8 mm, 4 mm, 2 mm, 1 mm, 0.5 mm, 0.25 mm, and 0.125 mm. Larger grain sizes (e.g. 32 mm) can be added to the model if they are present in the concrete. The transformation to a step-wise grain size distribution is done by dividing each aggregate fraction in two sizes. For example, the fraction between 8mm and 16mm is divided in one half of 8mm and one half of 16mm grains. ϕ_i is the fraction of each aggregate size in the total volume (see Fig.5).

2.1.2 Damage Evolution

The aggregate interlock effect degrades with increasing displacements. Each aggregate grain destroys the cement matrix in its contact zone and produces a lane in the sliding direction. However, the length of each lane is limited by the distance between the grains of the same size. Furthermore, the concrete cover and large parts of concrete between the reinforcement bars spall. Thus, a simplified damage evolution model D_i, a function of the sliding displacement, $u_{slid,I}$, is shown in Fig.7. This model is valid for each aggregate size for both the normal and the shear stresses at the crack (Eq. 4 and 5). The displacement, $u_{slid,i}$, is the sliding displacement of each aggregate size since the first contact, while u_{slid} is total differential sliding displacement between the two crack planes. It is assumed that the degradation starts when $u_{slid,start,i} = 0.5d_i$ and ends when $u_{slid,end,i} = 3.0d_i$ (see Fig.7).

Furthermore, the size of the initial crack width, w_0, affects the sliding resistance. Small aggregates do not participate in the aggregate interlock effect if the initial crack width is too large. This happens because aggregates with larger diameters destroy the sliding lanes of the smaller aggregates before they can interlock. Therefore, the aggregates with diameters smaller than half of the initial crack width are not considered.

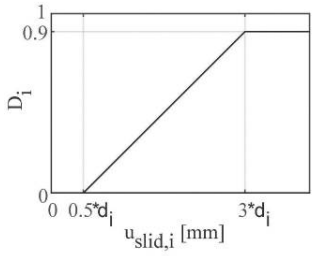

Fig.7 – Damage evolution along the sliding surface

The damage evolution law is applied for each aggregate grain size separately according to the following rule:

$$D_i = \begin{cases} 0.0 & \text{if} \quad u_{slid,i} \le 0.5 \cdot d_i \\ 0.36 \cdot \dfrac{u_{slid,i}}{d_i} - 0.18 & \text{if} \quad 0.5 \cdot d_i < u_{slid,i} \le 3.0 \cdot d_i \\ 0.9 & \text{if} \quad 3.0 \cdot d_i < u_{slid,i} \\ 1.0 & \text{if} \quad d_i \le \dfrac{w_0}{2} \end{cases} \tag{6}$$

The shear stress and the normal stress are considered to degrade in proportion to the damage. The resulting vertical and horizontal forces on the crack area, A_c, which are transferred by aggregate interlock, are modeled using Eq.(7) and Eq.(8), where $\overline{\tau_{c,i}}$ and $\overline{\sigma_{c,i}}$ are the stresses on the undamaged crack surface. n_d is the number of aggregate grain sizes, and ϕ_i is the fraction of the quantity of grain size, d_i, relative to the total. The factor, k, considers the ratio of the volume of the aggregates to the total volume of the concrete. The volume portions of the cement and the water do not contribute to the roughness at the crack. This ratio depends on many factors, but typical values are between 0.7 and 0.8. Here, the factor k is assumed to be 0.78.

$$F_{c,z}(u_{slide}, w) = \sum_{i=1}^{n_d} (1 - D_i) \cdot \overline{\sigma_{c,i}} \cdot \phi_i \cdot A_c \cdot k \tag{7}$$

$$F_{c,x}(u_{slide}, w) = \sum_{i=1}^{n_d} (1 - D_i) \cdot \overline{\tau_{c,i}} \cdot \phi_i \cdot A_c \cdot k \tag{8}$$

2.2 Deflection Model of the Reinforcement

The deflection model for the reinforcement bars crossing the crack is based on the assumption that the flexural stiffness of a reinforcement bar is small compared to its axial stiffness. Thus the flexural stiffness is neglected in this model. The second assumption is that the concrete enters a plastic response range when the reinforcement is laterally compressed into it. In Fig.8, this principle is applied to model the deflection of the reinforcement bars at the crack. Sliding displacements between two rigid concrete bodies forces the reinforcement to deform in double curvature (Fig.2). Only the bottom portion of the bar is shown in Fig. 8. This model considers that the reinforcement bars bend into an arc to match the sliding displacements along the crack (circular arc portion). At larger displacements, the concrete at the crack surface partially fails as a consequence of the indentation of the reinforcement into the concrete. The reinforcement bar above the crack is straight by inclined and is not supported by the concrete (inclined portion). The bottom section the reinforcement bar is straight, (straight portion). The change of the length of the reinforcement bar, which is controlled by the crack width and the radius of the arc, induces axial forces in the reinforcement bar.

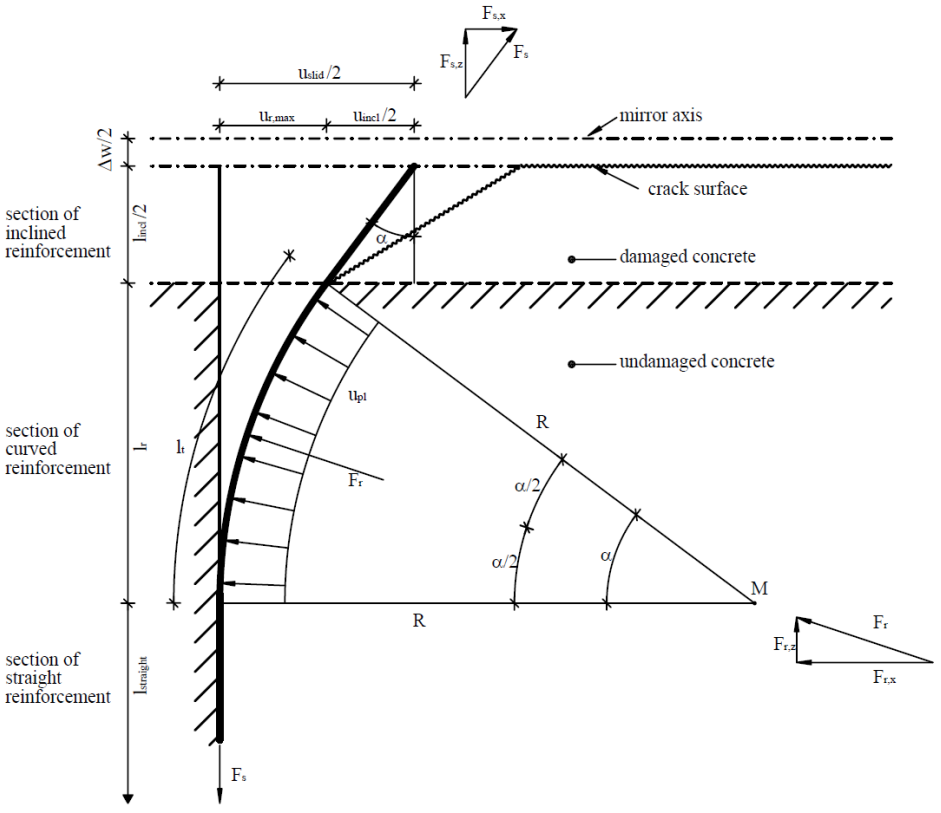

Fig.8 – Deflection model of the half of the reinforcement bar beneath the crack surface

Barlow's formula, given in Eq.(9), is applied to the curved section of the reinforcing bar. Namely, F/u=R, the longitudinal force divided by the distributed deflection force, u, gives the radius R of the circular arc of the bar. To simplify, it is assumed that the radius does not change during the sliding process. The yield force, F_y, of the reinforcement is inserted into Eq. (9) to ensures that the yield limit of the reinforcement bars is reached. The plastic distributed load, u_{pl}, is calculated in Eq.(10). The maximum plastic bearing stress of the concrete, $\sigma_{c,pl}$, is defined in Eq.(11). This assumption for the bearing strength is consistent with Souroushian [7] and Dulacska [8], where values between 1.2 and 3 times the uniaxial compression strength of the concrete are suggested.

$$R = F_y / u_{pl} \tag{9}$$

$$u_{pl} = \sigma_{c,pl} \cdot d_s \tag{10}$$

$$\sigma_{c,pl} = 4.0 \cdot f_c \tag{11}$$

The angle of the circular arc portion of the reinforcement, α, is equal to the inclination of the reinforcement bar at the crack. The angle, α, and the radius, R, define the transversal displacement of the concrete in the curved portion of the bar, u_r, see Eq.(12). This displacement is limited by $u_{r,max}$ (see Eq.(13)). The maximum displacement depends on the empirical assumption of Soroushian [7]. It describes the bearing stiffness of the concrete at a dowelled reinforcement bar.

$$u_r = R - R \cdot cos\alpha \leq u_{r,max} \tag{12}$$

$$u_{r,max} = \frac{\sigma_{c,pl}[N/mm^2]}{(127 \cdot \sqrt{f_c[N/mm^2]}) / d_s^{2/3}[mm]} \tag{13}$$

When the maximum displacement, $u_{r,max}$, is reached, the concrete fails locally. The reinforcement can freely deform in the inclined portion without any force transfer to the concrete. The sliding displacement consists of the curved portion displacement, u_r, and the inclined portion displacement, u_{incl}. In this model, u_{slid}, is an input parameter. Then Eq.(14) is solved for α and u_{incl}. Both parameters define the geometry of the reinforcement.

$$u_{slid} = u_{incl} + 2 \cdot u_r(\alpha) \tag{14}$$

The total length, l_{tot}, which is defined in Eq.(15), is the sum of the reinforcement bar lengths in the straight, curved, inclined portions, and the crack widths. $l_{straight}$ is calculated in Eq.(16), and the length of reinforcement in the curved portion of the bar l_t is analysed in Eq.(17). The height of the inclined portion of the bar, l_{incl}, is determined in Eq.(18). The crack width, w, is also taken into account, see Eq.(19). This includes the initial crack width, w_0, from prior load stages, which remains because of plastic elongation and the change of the crack widths, Δw. If the crack opens or closes, the length of the reinforcement changes, and this can result in positive or negative strain.

$$l_{tot} = 2 \cdot l_{straight} + 2 \cdot l_t + \frac{l_{incl}}{cos\ \alpha} + w \tag{15}$$

$$l_{straight} = \frac{l_{s,min}}{2} - \frac{l_{incl}}{2} - R \cdot sin\alpha \tag{16}$$

$$l_t = R \cdot \alpha[rad] \tag{17}$$

$$l_{incl} = \frac{u_{incl}}{tan\,\alpha} \tag{18}$$

$$w = w_0 + \Delta w \tag{19}$$

The length, $l_{straight}$, depends on the minimal crack space, $l_{s,min}$, defined in Eq.(20), which is the half of the maximum crack space (see Eq.(21)). This length is calibrated using the data from the conducted sliding tests to obtain a good match of the change of the crack widths. The bond strength for the calculation of the maximum crack space is taken from the CEB-FIB Model Code 90 [9].

$$l_{s,min} = \frac{1}{2} \cdot l_{s,max} \tag{20}$$

$$l_{s,max} = \frac{f_{ct,eff} \cdot (1-\rho_s) \cdot d_s}{2 \cdot 1.8 \cdot f_{ct,eff} \cdot \rho_s} \tag{21}$$

The strain analysis is shown in Eq.(22), with the simplification that the bond stress does not reduce the longitudinal stress in the bar. This means that the strain inside the reinforcement is constant over the length l_{tot}.

$$\epsilon_s = \frac{l_{tot} - l_{s,min}}{l_{s,min}} \tag{22}$$

The longitudinal stress-strain behaviour of the reinforcement is defined using a linear-plastic material law with the elastic modulus, E_s, the yielding strength, f_y, and the ultimate strain ε_u. The axial force of all reinforcement bars, F_s, is calculated from the Eq.(23). Subsequently the force is decomposed into a force normal to the crack plane, $F_{s,z}$, and a force parallel to the crack plan, $F_{s,x}$, (see Eq.(24) and Eq.(25) 4.29). The reinforcement forces depend on the sliding displacement, u_{slid}, and are solved for the crack width, w.

$$F_s = \sigma_s(\epsilon_s) \cdot A_s \tag{23}$$

$$F_{s,x}(u_{slid}, w) = F_s(\alpha, w) \cdot sin\alpha \cdot n_s \tag{24}$$

$$F_{s,z}(u_{slid}, w) = F_s(\alpha, w) \cdot cos\alpha \cdot n_s \tag{25}$$

Fig.9 shows the reinforcement bar deflection process under increasing sliding displacements with constant crack widths. In phase 0, no sliding displacements exist. The elastic strain in the reinforcement bar is zero. The plastic strain results from a crack opening that elongates the bar into its plastic range. In phase 1a, with small transverse displacements, the inclination angle α is small as is the curved portion of the bar. In phase 1b, the inclination angle increases to remain compatible with the increasing sliding displacements. During this process, the reinforcement bar deforms into the concrete. In phase 2, the maximum bearing displacement is, $u_{r,max}$, is reached. The concrete starts to partially fail, and the midpoints of the curved sections move away from the crack. As the displacement process proceeds further, the reinforcement can yield. In all phases, the strain of the reinforcement is calculated, by Eq.(22). The reinforcement bar transfers axial forces and no shear forces at its local coordinate system. This means that dowel action is neglected. However, due to the inclination of the bars, shear forces are transferred to the crack plane. The equilibrium of the reinforcement bar axial force, F_s, with components $F_{s,x}$ and $F_{s,z}$, is equilibrated by the concrete F_r (see Fig.8) with components $F_{r,x}$ and $F_{r,z}$. The horizontal equilibrium is achieved when $F_{s,x} = F_{r,x}$, and the vertical equilibrium is achieved when $F_s = F_{r,z} + F_{s,z}$.

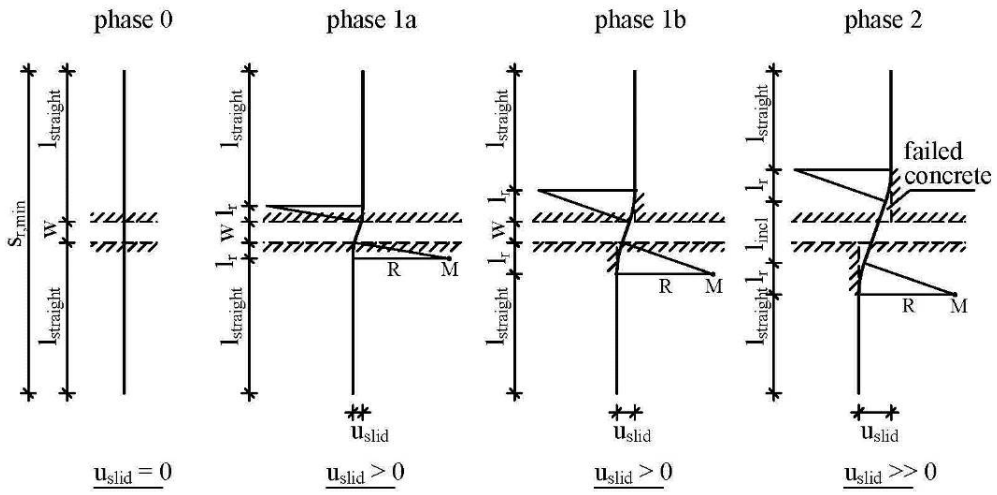

Fig.9 – Deflection process

2.3 Solving the Sliding Force-Displacement Relationship

An input parameter for the sliding model is the angle of the compression strut, β, in the wall (see Fig.3). This angle can vary between 0° and 90°. The angle β determines the ratio between the external normal force, F_z, and the shear force, F_x, and thereby the direction of the resultant force, which is transferred across the crack (see Eq.(26)).

$$tan\beta = \frac{F_z(u_{slid}, w)}{F_x(u_{slid}, w)} \tag{26}$$

The external forces are in equilibrium with the internal forces (concrete and reinforcement) in each direction. This leads to Eq.(27) and Eq.(28).

$$F_z = F_{c,z}(u_{slid}, w) + F_{s,z}(u_{slid}, w) \tag{27}$$

$$F_x = F_{c,x}(u_{slid}, w) + F_{s,x}(u_{slid}, w) \tag{28}$$

The deflection model of the reinforcement and the aggregate interlock model for the concrete depend on the displacement, u_{slid}, and the crack width, w. To solve Eq.(27) and Eq.(28) for the shear-force sliding relation, Eq.(26) is used. The angle, β, is predefined to solve Eq.(26) for w. If w is known for the deformation state, u_{slid}, the forces of the concrete ($F_{c,x}$, $F_{c,z}$), and the reinforcement ($F_{s,x}$, $F_{s,z}$) are calculated. This procedure is repeated in every sliding displacement step, u_{slid}. The load history of the reinforcement is considered.

3. Calibration

The sliding model is calibrated using the data from the experiments conducted in this project [10]. Most of tests were conducted cyclically. It was shown that the monotonic load-displacement response curve is an envelope function for the cyclic response graph. Thus, the model is calibrated to the monotonically tested specimens out of the core group, PK05 and PK11. For calibration of the sliding model the following parameters are set:

- damage evolution law, $u_{slid,start,i} = 0.5d_i$, $u_{slid,end,i} = 3.0d_i$ (see Fig.7);
- maximum compression bearing strength of the reinforcement, $\sigma_{c,pl} = 4.0f_c$ (see Eq.(11));
- considered crack space, $l_{s,min} = 0.5l_{s,max}$ (see Eq.(20)).

These parameters are varied in Fig.10. The black solid line shows the response of the sliding model using the above chosen parameters.

The empirical damage evolution law is part of the aggregate interlock model and describes the post peak behaviour (see Fig.7). In Fig.10, the damage evolution law is also varied. The response when the damage evolution law starts to degrade at $u_{slid,start,i} = 1.0d_i$, and ends at $u_{slid,end,i} = 6.0d_i$ is plotted using a blue dashed line. The response when the damage evolution law starts to degrade at $u_{slid,start,i} = 0.25d_i$, and ends at $u_{slid,end,i} = 1.5d_i$ is plotted as a blue dot-dashed line. The sliding shear stress-displacement relationship is significantly affected by this law. A delayed degradation process leads to a higher maximum resistance, and the maximum resistance is reached at a larger sliding displacement. The opposite is the case for an earlier starting and an earlier ending degradation process: it leads to lower shear stresses at smaller sliding displacements. The influence on the change of the crack width is negligible (see Fig.10).

The maximum compression bearing strength of the reinforcement, which is defined in Eq.(11), influences the force-deformation behaviour of the reinforcement. In this study $\sigma_{c,pl}$ is varied between $3.0f_c$ and $5.0f_c$. The comparison of the different green-line plots shows that an increase of the bearing stress leads to an increase of the shear stresses. The reason is the different crack closure processes. An increase of the bearing strength reduces the radius of the curved portion of the reinforcement bar. At the same sliding displacement, the reinforcement with a larger plastic bearing strength lengthens more, and this produces higher clamping forces. To fulfill the force equilibrium, the crack closes (see Fig.10), and thus increases the aggregate interlock effect.

The crack space considered is varied between $l_{s,min} = 0.25l_{s,max}$ and $l_{s,min} = 1.00l_{s,max}$. The influence of the considered crack space is very small (see the red lines). With a smaller length, the shear stresses are larger. This results from the crack closure process that differs during the first 10 mm of sliding displacement. The sliding model with the chosen parameters closely matches the measured results of PK05 and PK11.

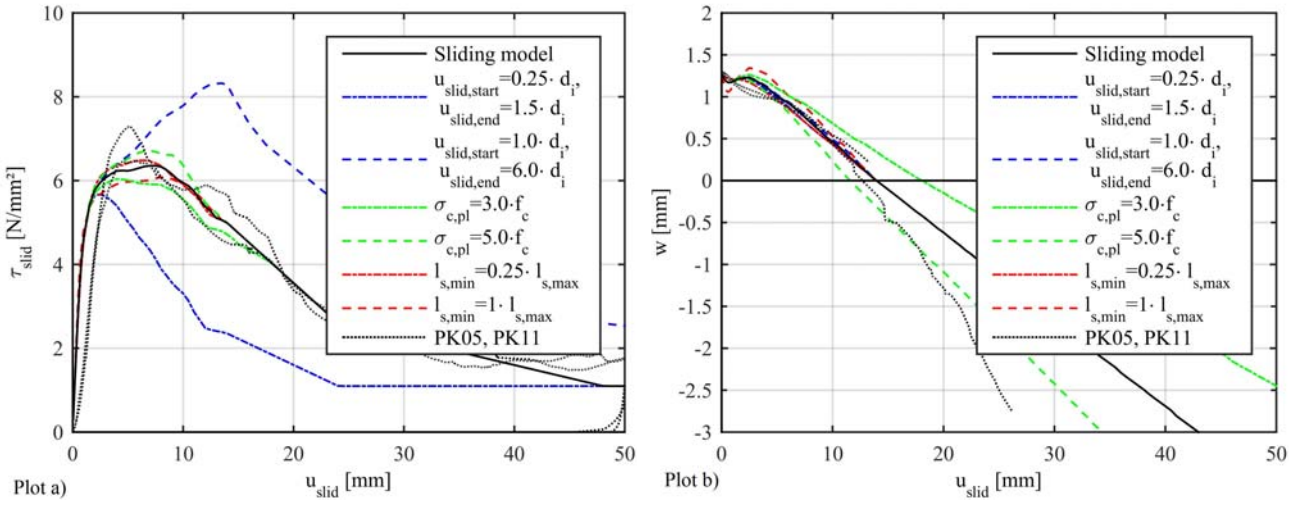

Fig.10 – Calibration of the sliding model against specimens PK05 and PK11, ρ_s=0.85%, w_0=1.28mm, ds=8mm

4. Validation

The sliding model is validated using data from specimens PK09, PK10, PK17, PK18, PK21, and PK22 [10]. These tests are conducted in the same test setup used for specimens PK05 and PK11, which were used to calibrate of the model. These specimens differ in their reinforcement ratios, ρ_s, and their initial crack width, w_0. Furthermore, these tests are conducted using a cyclic load sequence, while the sliding model describes a monotonic sliding shear stress-displacement relationship across a crack.

The reinforcement ratio, ρ_s=1.13%, of the specimens PK17 and PK18 is larger compared to that of the core group, ρ_s=0.85%. The higher reinforcement ratio leads to a faster crack closure process. Because of this, the sliding resistance of the model, τ_{slid}=6.7 N/mm², is reached at u_{slid}=6 mm, this equal to the measured average maximum shear resistance for PK17 and PK18. Overall Fig.11 shows a good match between the tests and the model.

The load-displacement behaviour of specimens PK21 and PK22, with a lower reinforcement ratio, ρ_s=0.47%, also show good agreement with the predictions of the sliding model (see Fig.12). The sliding model predicts a sliding resistance of τ_{slid}=5.7 N/mm² at u_{slid}=9 mm, and the specimens reached their maximum resistance, τ_{slid}=6.7 N/mm², at u_{slid}=10 mm.

The specimens PK09 and PK10 were initially cracked with a crack width of 1.0 mm. After load removal, an average crack width of 0.35mm remained. The reinforcement ratio is ρ_s=0.85%. The sliding resistance of the model is 9.1 N/mm², while the average maximum sliding shear stress is 9.85N/mm². The measured load-deformation behaviour is similar to the predicted one. In Fig.13, the plots of the specimens and the model response show the same characteristics. Overall, the sliding model can predict the load-deformation behaviour of the compact sliding specimens with acceptable accuracy.

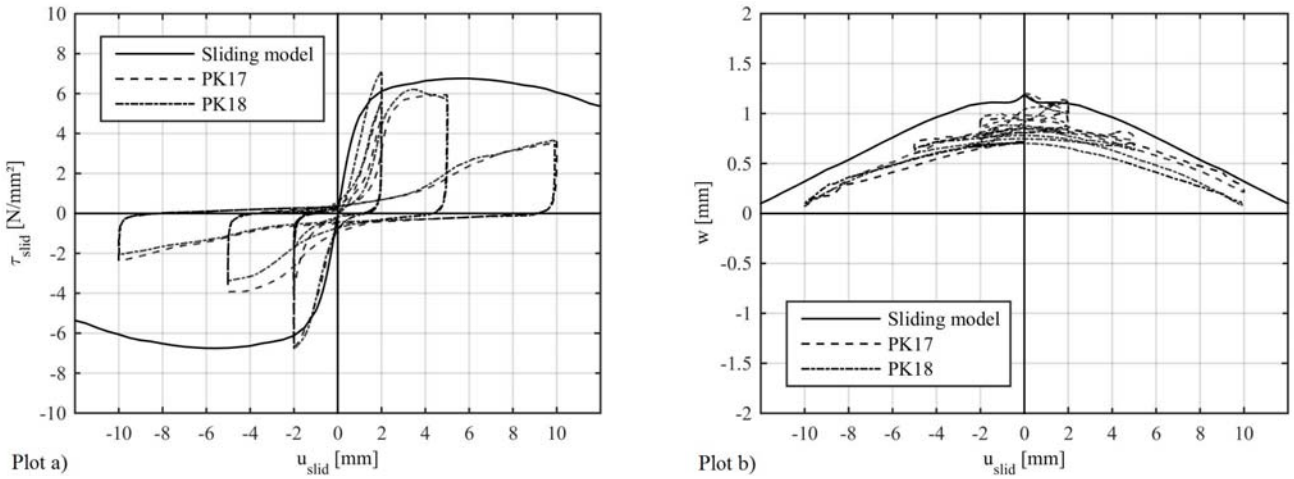

Fig.11 – Sliding model prediction of the response of specimens PK17 and PK18, ρ_s=1.13%, w_0=1.13mm, d_s=8mm

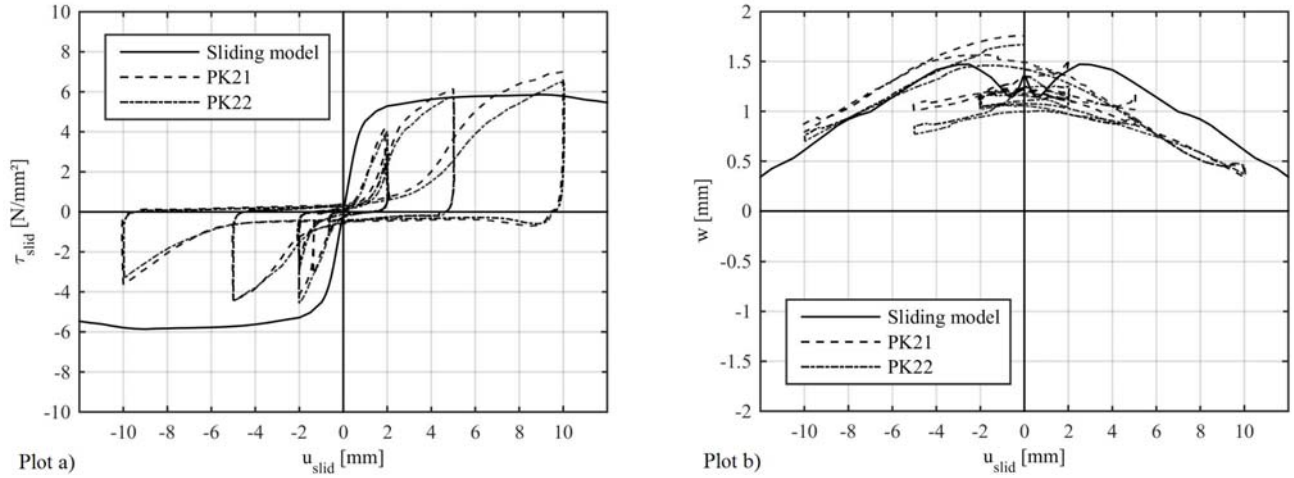

Fig.12 – Sliding model prediction of the response of specimens PK21 and PK22, ρ_s=0.47%, w_0=1.38mm, d_s=6mm

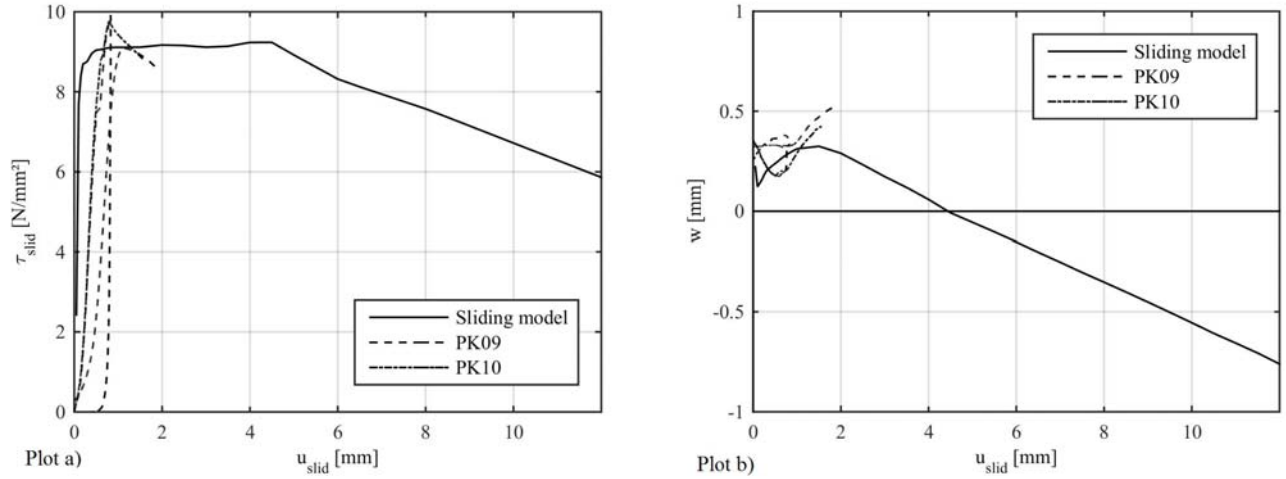

Fig.13 – Sliding model prediction of the response of specimens PK09 and PK10, ρ_s=0.85%, w_0=0.35mm, d_s=8mm

5. Conclusion

The sliding model proposed in this study comprises two parts, the aggregate interlock mechanism of the concrete and the deformation mechanism of the reinforcement. The aggregate interlock part depends mainly on the roughness of the crack surface and the concrete strength. The force transfer of the reinforcement depends mainly on the reinforcement ratio, ρ_s, and the diameter of the reinforcement bars, d_s. Both parts contribute to the shear and axial force transfer across the crack. They are related through the compatibility of deformations, the sliding displacement, u_{slid}, and the crack width, w. The angle of the resultant wall compression strut, β, is predefined. Then, the equilibrium of forces for the crack width, w, is solved for each increment of the sliding displacement.

The model is calibrated using response data from the monotonically tested compact sliding specimens, PK05 and PK11 and validated using the response data from the cyclically tested specimens with different reinforcement ratios and different initial crack widths. The load-deformation response predicted using the sliding model matches the test results well. The results of the model and the tests are strongly influenced by the initial crack width, w, while the influence of the reinforcement on the sliding response is small.

The next step of the research project incorporates the sliding model into a model of a wall to predict the load-deformation behaviour of squat shear walls including the sliding on the bottom flexural crack.

6. References

[1] Nagae T, Ghannoum WM, Kwon J, Tahara K, Fukuyama K, Matsumori T et al (2015): Design Implications of Large-Scale Shaking Table Test on Four-Story Reinforced Concrete Building. *ACI Structural Journal,* (**112**), 135–146.

[2] Whyte CA, Stojadinovic B (2013): *Hybrid Simulation of the Seismic Response of Squat Reinforced Concrete Shear Walls*. Pacific Earthquake Engineering Research Center Headquater at the University of California, Berkeley, USA.

[3] Synge AJ, Priestley MJN, Paulay T (1980): *Ductility of squat shear walls*. Dept of Civil Engineering, University of Canterbury, New Zealand.

[4] Luna BN, Rivera JP, Whittaker AS (2015): Seismic Behavior of Low-Aspect-Ratio Reinforced Concrete Shear Walls. *ACI Structural Journal,* **112**(5).

[5] Walraven JC, Reinhardt HW (1981): *Theory and experiments on the mechanical behaviour of cracks in plain and reinforced concrete subjected to shear loading*. Delft.

[6] DIN Deutsches Institut für Normung e.V. *Concrete, reinforced and prestressed concrete structures - Part 2 - Specifications, properties, production and conformity - Application rules for DIN EN 206-1*(**DIN 1045-2**). Beuth Verlag GmbH, Berlin.

[7] Soroushian P, Obaseki K, Ronjas MC (1987). Bearing Strength and Stiffness of Concrete Under Reinforcing Bars. *ACI Materials Journal,* **84**(3).

[8] Dulacska H (1972): Dowel Action of Reinforcement Crossing Cracks in Concrete. *ACI Journal Proceedings,* **69**(12).

[9] CEB-FIP model code 1990 (1993): Design code. London, Telford.

[10] Trost B, Schuler H, Stojadinovic B (2014): Experimental investigation of sliding on compact sliding specimens under cyclic loads. *Proceedings of the 15th European Conference on Earthquake Engineering*. Istanbul.